Atomic Structure of the Passive Oxide Film Formed on Iron

Michael F. Toney
Almaden Research Center, IBM Research Division, 650 Harry Road, San Jose, California 95120

Alison J. Davenport,* Lucy J. Oblonsky,† Mary P. Ryan, and Carissima M. Vitus‡
Department of Applied Science, Brookhaven National Laboratory, Upton, New York 11973-5000
(Received 14 July 1997)

We have used x-ray scattering to measure the structure of the passive oxide film formed at high anodic potentials on Fe(110) and Fe(001). The crystalline film has a small crystallite size (≈50 Å) and is oriented with the substrate. The film structure is based on Fe_3O_4, but with cation vacancies on octahedral and tetrahedral sites (80% and 66% occupancies, respectively) and with cations occupying octahedral interstitial sites (12% occupancy). These results resolve the long-standing controversy surrounding the film structure and provide a basis for understanding and modeling film properties important for corrosion resistance. [S0031-9007(97)04600-0]

PACS numbers: 81.65.Rv, 61.10.–i, 68.55.–a, 81.65.Mq

As the applied potential of iron in aqueous solution is slowly changed from negative (cathodic) to positive (anodic), the iron first begins to dissolve, but at a sufficiently anodic potential, a thin (≈30 Å) oxide film forms and prevents further dissolution. This is known as passivity and is illustrated in Fig. 1. This phenomenon was discovered in the 1700s and has been extensively investigated since then [1]. However, despite decades of research, there is little agreement on the atomic structure of this passive film. Electron diffraction and electrochemical experiments [2–4] led to the suggestion that the film consists of an inner layer of Fe_3O_4 and an outer layer of γFe_2O_3. However, since the electron diffraction measurements were conducted *ex situ* (the iron electrode was removed from the electrolyte) and in vacuum, the film may have been altered through crystallization and/or removal of OH. These concerns led to studies of the passive film on iron using a variety of *in situ* techniques (where the film is measured in the environment where it was grown), for example, Mössbauer spectroscopy [5,6], extended x-ray absorption fine structure [7–9], and surface enhanced Raman scattering [10,11]. These were interpreted, in contrast, as showing that the passive film is amorphous and/or similar to Fe hydroxides or oxyhydroxides. However, recent *in situ* x-ray absorption near-edge structure data suggest that the film is either amorphous or a spinel (similar to Fe_3O_4 or γFe_2O_3) [12], and *in situ* scanning tunneling microscopy (STM) measurements suggest that the film is crystalline and consistent with Fe_3O_4 or γFe_2O_3 [13]. To resolve this long-standing controversy, *in situ* and *ex situ* x-ray diffraction and STM were used to determine the passive film structure at a high anodic formation potential.

The widespread disagreement on the passive film structure is partly due to the difficulty in characterizing the film: measurements must be conducted *in situ*, and the film is thin. Disagreement regarding the film structure has been exacerbated by the variety of film formation methods. We used a method that results in no dissolution of Fe [12,14], avoiding the production of ferrous ions and subsequent reprecipitation of iron oxyhydroxide. The iron crystals were immersed in pH 8.4 borate buffer at −1.4 V, and the air-formed oxide was removed by cathodic reduction at −1.8 V for 10–60 min and then −1.4 V for 20 min (all potentials are quoted relative to mercurous sulfate electrode). The passive film was formed by stepping to 0.4 V and maintaining this potential for 60 min. *In situ* data were obtained with the potential continuously held at 0.4 V, while for the *ex situ* experiments, the electrode was emersed and placed in flowing high purity He gas. We collected extensive data sets *ex situ*, where there was no background x-ray scattering from the electrolyte and we could measure many diffraction peaks. We then obtained *in situ* data for comparison. This allowed us to determine that the passive film was not altered upon removal from the electrolyte,

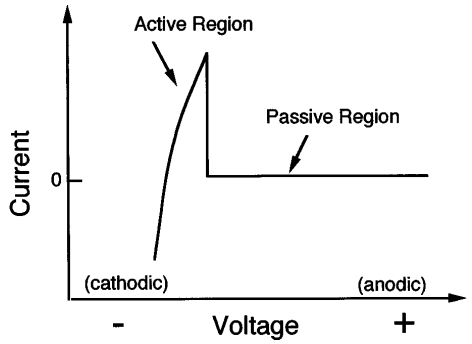

FIG. 1. Idealized current potential curve for a passivating metal. As the potential is slowly increased from cathodic to anodic, the metal exhibits an active region where it freely dissolves. However, at a critical potential, a passive film forms, which protects the metal from further corrosion and results in a drastically lower current.

 0031-9007/97/79(21)/4282(4)$10.00

and thus, we could use the *ex situ* data set for a crystallographic analysis of the film structure.

Figure 2 shows the measured diffraction patterns from the passive film on Fe(001) and Fe(110). For clarity, only part of the patterns is shown. The epitaxy of the passive film is apparent from Fig. 2. For growth on Fe(001), the oxide(001) planes lie parallel to the iron surface, while for Fe(110), the oxide(111) planes are parallel to the surface. For both crystal surfaces, the oxide$[\bar{1}10]$ direction is parallel to Fe[100]. This orientational relationship is apparently fixed by the similarity between the oxide$(\bar{2}20)$ and Fe(100) plane spacings (2.96 and 2.89 Å, respectively). Based on the measured lattice parameters (Fig. 2), the symmetry, and a qualitative assessment of the diffraction intensities, the x-ray data are consistent with those of spinel oxides (γFe_2O_3, Fe_3O_4, or related structures).

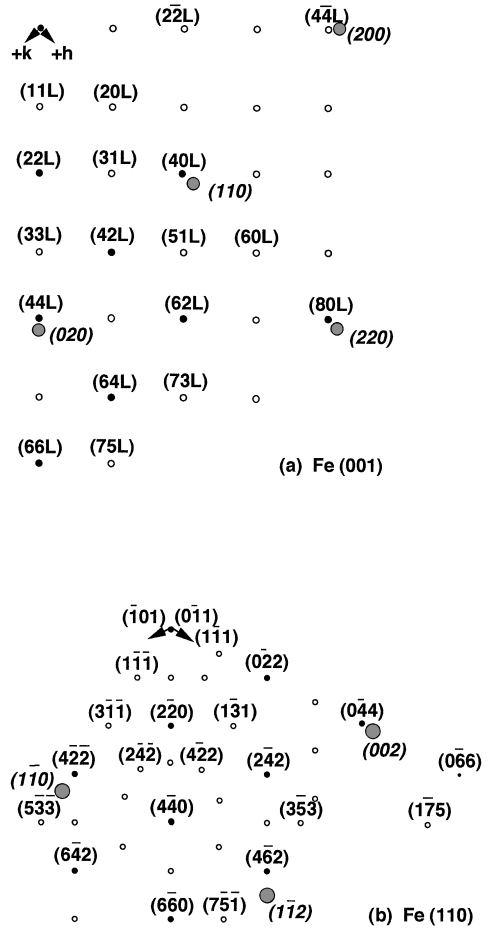

FIG. 2. One quadrant of the diffraction pattern for the passive film on (a) Fe(001) and (b) Fe(110). For clarity, only some of the measured out-of-plane peaks are shown. In (a) these are collectively denoted by "L." The diffraction peaks from the oxide are represented by small filled and open circles (which are purely in-plane peaks and peaks that are nearly in plane, respectively). Substrate peaks are represented by the large, lightly shaded circles. The lattice constants of the film are $a_0 = 8.39 \pm 0.01$ and 8.3 ± 0.1 Å, parallel and perpendicular to the substrate surface, respectively.

They are inconsistent with other crystalline bulk iron oxides, hydroxides, or oxyhydroxides. We also searched for other such bulk phases (with both x-ray diffraction and STM) but did not detect the presence of any other phase.

Before describing the crystallography, it is important to demonstrate that the structure of the passive film is not altered on emersion. Figure 3 shows *in situ* and *ex situ* structure factors for some of the reflections from the film.

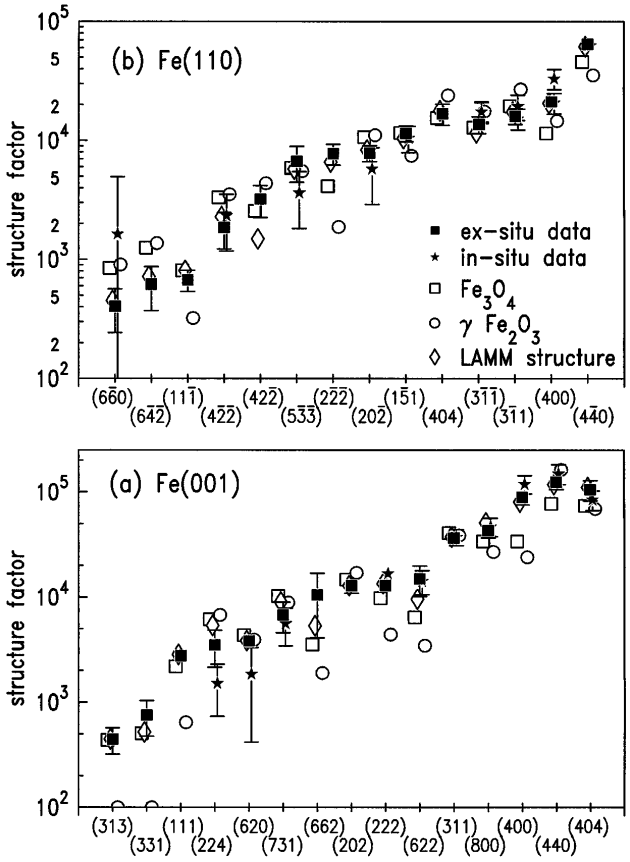

FIG. 3. Measured and best-fit structure factors for a subset of the diffraction peaks for the passive film grown on (a) Fe(001) and (b) Fe(110). Data are shown by the solid symbols (*in situ* by squares and *ex situ* by stars) and were calculated from the integrated intensities of the diffraction peaks. The *ex situ* data have been (approximately) converted into electron units, while the *in situ* data have been corrected for x-ray absorption by the x-ray cell [22]. Error bars represent one sigma errors. The best fits for the model structures are the open symbols. In the fits to the data for γFe_2O_3 (open circles) and Fe_3O_4 (open squares), we allowed six scale factors to vary (in-plane and out-of-plane data sets for three different experiments). For the passive film structure (which we call the LAMM phase, open diamonds), four additional parameters are required: occupancies of the Fe octahedral and tetrahedral sites and concentration of the octahedral and tetrahedral interstitials, although the best-fit tetrahedral interstitial concentration was zero. The iron and oxygen ions were fixed in the ideal sites for a spinel. The lateral Debye-Waller factor for the Fe cations was varied in the range $\sigma_{\parallel}(\mathrm{Fe}) = 0.1 - 0.15$ Å, while the other Debye-Waller factors were fixed as $\sigma_{\perp}(\mathrm{Fe}) = 0.28$ Å, $\sigma_{\parallel}(\mathrm{O}) = 0.1$ Å, and $\sigma_{\perp}(\mathrm{O}) = 0.28$ Å.

As is evident, there is excellent agreement between the *in situ* and *ex situ* data. Furthermore, specific diffraction scans show complete agreement for the peak shapes and widths. These results show that, for the passive film formed at high anodic potentials, the structure is not altered by emersion.

Some previous results suggested that the passive film on iron is amorphous or partially amorphous [5,7–9,11]. Our results rule out a purely amorphous film, but the film could be partly amorphous. The x-ray data do not show any indication of an amorphous oxide or oxyhydroxide. However, to further test for the presence of such a film, we used STM, which shows there is a crystalline layer at the passive film surface, consistent with Ref. [13]. Thus, the amount of amorphous material in the passive film is less than our detectability limits ($\approx 5\%$).

To deduce the passive film structure, the diffraction peak intensities of 101 peaks were converted into structure factors and reduced to 68 symmetry inequivalent peaks. These were then compared with candidate structures: Fe_3O_4 and γFe_2O_3, as suggested by previous investigators. Our data demonstrate that neither Fe_3O_4, γFe_2O_3, nor any combination of these phases can adequately describe the experimental data. This is evidenced by Fig. 3, where we show the expected structure factors for Fe_3O_4 and γFe_2O_3. Many of the expected structure factors are well outside the experimental error [for example, the (222), (622), (400), (440), and (404) in Fig. 3(a) and the $(6\bar{4}\bar{2})$, $(2\bar{2}\bar{2})$, (400), and $(4\bar{4}0)$ in Fig. 3(b)]. Furthermore, the goodness-of-fit parameters are unacceptably large, $\chi^2 = 7.3$ and 4.2 for γFe_2O_3 and Fe_3O_4, respectively. This unambiguously establishes that these phases are *not* present in the passive film on iron.

To determine the correct passive film structure, we first note that the lattice constants of the film are close to those of bulk Fe_3O_4 and γFe_2O_3. Since the lattice constants of spinel oxides are predominantly determined by the packing of oxygen anions [15], this suggests that all the oxygen sites are fully occupied. However, cation vacancies and interstitials in spinels have a low free energy of formation [16], and thus, we considered models with random cation vacancies and interstitials (Fig. 4). We find that such a model fits the experimental data very well. The model structure factors are shown by the open diamonds in Fig. 3, and with only a couple of exceptions, they are within the error bars of the data. Furthermore, the vacancy-interstitial model has $\chi^2 = 1.3$, demonstrating its validity.

The spinel unit cell contains 32 oxide anions, and 16 octahedral and 8 tetrahedral cation sites [15,17]. In Fe_3O_4 these sites are fully occupied, while in γFe_2O_3, 25% of the octahedral sites have a 33% occupancy, and the other octahedral sites and all the tetrahedral sites are fully occupied. These spinels contain no interstitials. The structure of the passive film (Fig. 4) has an octahedral site occupancy of $(80 \pm 10)\%$ and a tetrahedral site occupancy of $(66 \pm 10)\%$; there are cations occupying

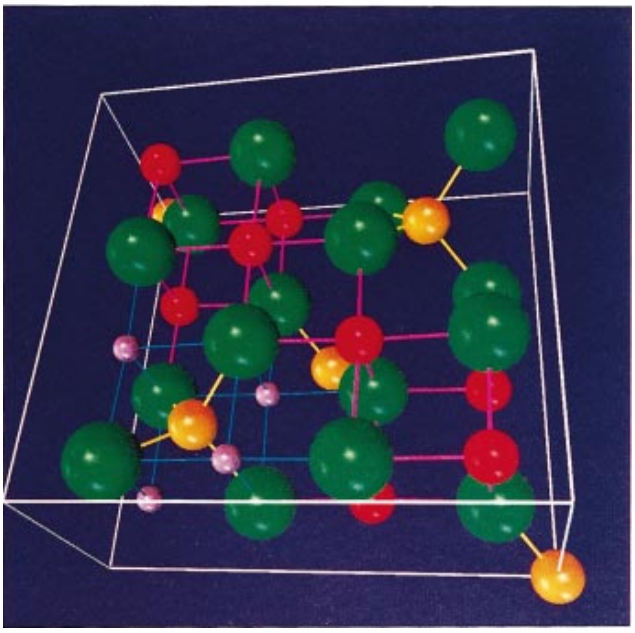

FIG. 4(color). Schematic illustration of the passive film (LAMM) structure. For clarity, only the bottom half of the unit cell is shown and is outlined by the solid white lines. The oxygen anions are shown by the large green spheres (fully occupied), the tetrahedral cation sites by smaller orange spheres (66% occupancy), and the octahedral cation sites by red spheres (80% occupancy). Four of the eight octahedral interstitial sites are shown by the small purple spheres; there are four equivalent sites at the upper right hand section, which are not shown. Note that for clarity the interstitials are shown in ordered positions; in our model (LAMM) structure they are assumed to be randomly distributed. The bonds are illustrated by the lines: yellow for tetrahedral, magenta for octahedral, and blue for the octahedral interstitials.

$(12 \pm 4)\%$ of the available octahedral interstitial sites, but no tetrahedral interstitials [18]. It is likely that there is a correlation between the tetrahedral vacancies and the octahedral interstitials: these interstitial cations have a high probability of occupying sites near tetrahedral vacancies. On the other hand, it is also likely that the interstitials will predominate closer to the metal-oxide interface and the vacancies closer to the oxide-solution interface, since the iron cations are probably in a higher oxidation state closer to the electrolyte. However, such a distinction is not possible with our present data; our model (LAMM phase) assumes a uniform distribution of vacancies and interstitials. The stoichiometry for the best-fit structure, $Fe(1.9 \pm 0.2)O(3)$, indicates that most of the Fe cations are in the Fe(3+) state, consistent with previous results [12,14,19]. We emphasize that the LAMM phase is different from the proposed duplex $\gamma Fe_2O_3/Fe_3O_4$ film [2–4]. First, the octahedral vacancies are randomly distributed in the LAMM phase, but occupy specific sites in γFe_2O_3 and are absent in Fe_3O_4; and second, in γFe_2O_3 and Fe_3O_4, the tetrahedral sites are fully occupied and there are no octahedral interstitials.

From the diffraction peak widths, we find that the lateral crystallite size of the passive film is ≈60 and ≈45 Å for growth on Fe(001) and Fe(110), respectively. These are small crystallites, and thus, the passive film is best characterized as nanocrystalline. The peak-width data also show that the oxide has numerous planar defects, principally stacking faults and antiphase boundaries. The Debye-Waller factors in the passive film are large (0.1–0.15 and 0.28 Å, parallel and perpendicular to the surface; see Fig. 3 for details). This is due to static disorder in the atomic positions resulting from bond-length variations caused by the vacancies and interstitials.

In addition to resolving the long-standing question about the passive film structure, our results have other implications. For example, the corrosion resistance of the passive film is influenced by its ionic and electronic transport properties, which are largely determined by the film's crystallographic structure, and its defects and microstructure [20]. Our explicit description of these opens the way to detailed modeling of these properties. On the other hand, the most common engineering approaches to corrosion protection involve adding alloying elements to the metal (stainless steel) or inhibiting chemicals to aggressive environments. Our results on iron provide a starting point for understanding how these approaches affect passive films and provide enhanced corrosion protection. Additionally, the passive film microstructure is nanocrystalline, and such solids are increasingly recognized as having mechanical properties (e.g., hardness and ductility) that are distinctly better than bulk solids [21]. By conferring mechanical robustness, the film's nanocrystalline nature may be important for its corrosion resistance.

This work was performed at the National Synchrotron Light Source, beam line X20A. We thank Jean Jordon-Sweet for assistance with X20A, Chi-Chang Kao for the generous use of his detector, Ruediger Dieckmann for useful electronic discussions, and Joe Hriljac for initial assistance with data analysis. This work was performed partly under the auspices of the U.S. DOE, Division of Materials Science, Office of Basic Energy Sciences, under Contract No. DE-AC02-76CH00016.

*Present address: Manchester Materials Science Centre, University of Manchester/UMIST, Manchester M1 7HS, UK.

†Present address: DuPont Central Research and Development, P.O. Box 80323, Wilmington, DE 19880-0323.

‡Present address: MEMC Electronics, 501 Pearl Dr., St. Peters, MO 63376.

[1] H. H. Uhlig, in *Passivity of Metals*, edited by R. P. Frankenthal and J. Kruger (The Electrochemical Society, Inc., Princeton, NJ, 1978), p. 1.
[2] M. Nagayama and M. Cohen, J. Electrochem. Soc. **109**, 781 (1962).
[3] C. L. Foley, J. Kruger, and C. J. Bechtoldt, J. Electrochem. Soc. **114**, 994 (1967).
[4] K. Kuroda *et al.*, J. Electrochem. Soc. **129**, 2163 (1982).
[5] W. E. O' Grady, J. Electrochem. Soc. **127**, 555 (1980).
[6] J. Eldridge and R. W. Hoffman, J. Electrochem. Soc. **135**, 955 (1989).
[7] M. Kerkar, J. Robinson, and A. J. Forty, Faraday Discuss. Chem. Soc. **89**, 31 (1990).
[8] G. G. Long, J. Kruger, D. R. Black, and M. Kuriyama, J. Electroanal. Chem. **150**, 603 (1983).
[9] R. W. Hoffman, in *Passivity of Metals and Semiconductors*, edited by M. Froment (Elsevier Science Publishers B.V., Amsterdam, 1983), p. 147.
[10] J. C. Rubim and J. Dünnwald, J. Electroanal. Chem. **258**, 327 (1989).
[11] J. Gui and T. M. Devine, Corros. Sci. **32**, 1105 (1991).
[12] A. J. Davenport and M. Sansone, J. Electrochem. Soc. **142**, 7254 (1995).
[13] M. P. Ryan, R. C. Newman, and G. E. Thompson, J. Electrochem. Soc. **142**, L177 (1995).
[14] L. J. Oblonsky *et al.*, J. Electrochem. Soc. **144**, 2398 (1997).
[15] R. W. Wyckoff, *Crystal Structures* (Interscience Publishers, New York, 1965), Vol. 3.
[16] R. Dieckmann, Solid State Ion. **12**, 1 (1984).
[17] G. A. Waychunas, in *Oxide Minerals: Petrologic and Magnetic Significance*, edited by D. H. Lindsley (Mineralogical Society of America, Chelsea, MI, 1991), p. 11.
[18] The error bars were calculated by determining the occupancies that doubled the best fit χ^2.
[19] B. M. Buechler *et al.*, Electrochem. Soc. Proc. **96-18**, 172 (1996).
[20] C. Wagner, Ber. Bunsen-Ges. Phys. Chem. **77**, 1090 (1973).
[21] R. W. Siegel, Nanostruct. Mater. **3**, 1 (1993).
[22] M. F. Toney *et al.*, Phys. Rev. B **42**, 5594 (1990).